RESEARCH ARTICLE
PLANETARY SCIENCES

Earth and Planetary Physics
10: 315–325, 2026
doi: 10.26464/epp2026023

Influence of Martian environmental variables on methane partial pressure estimation

FengYi Chen, and Rui Li*

University of Science and Technology of China, School of Earth Space and Science, Hefei 230026, China

Key Points:

- Analysis of correlations between methane concentrations and multiple environmental variables in Mars' Gale Crater was conducted.
- The seasonal methane cycle in Gale was successfully reconstructed using the method of Fuller et al., 1966.
- Although previous studies have modeled the methane flux from Ultraviolet (UV) radiation-induced photolysis of organic materials on Mars, these studies lack support from actual surface UV radiation measurements. We used REMS/UVC data for our simulations.
- Cross-validation of several potential physical models was performed to verify their plausibility.

Citation: Chen, F. Y., and Li, R. (2026). Influence of Martian environmental variables on methane partial pressure estimation. *Earth Planet. Phys.*, *10*(2), 315–325. http://doi.org/10.26464/epp2026023

Abstract: Methane is considered a potential biosignature gas. The Mars Science Laboratory (MSL) Curiosity rover has observed seasonal variations in atmospheric methane within Gale Crater, suggesting possible microbial activity. The origin of this methane could be either biological or abiotic or a combination of the two. Different physical mechanisms, involving distinct environmental variables, produce varying concentrations of methane. By analyzing the influence of various environmental variables on methane partial pressures and comparing differences between physical models and empirical measurements, we can better discern methane production mechanisms. This study investigates factors affecting methane cycling. We find that temperature and pressure strongly correlate with Martian atmospheric methane, while Ultraviolet (UV) radiation at the atmospheric boundary and surface UV radiation exhibit weaker correlations. Using Fuller's method, we successfully reproduce the seasonal methane cycle in Gale Crater. Several potential physical models suggest that gas diffusion driven by variations in pressure and temperature within the shallow subsurface regolith may represent a primary mechanism determining methane concentrations observed in Gale Crater. However, errors in the pressure-dominated model cannot be neglected. As Curiosity enters its uphill exploration phase, we suggest that atmospheric pressure will play a significant role in predicting the methane concentrations that it will detect.

Keywords: methane; Fuller's method; air pressure

1. Introduction

A primary scientific objective in exoplanet research is the identification of potentially habitable worlds. Atmospheric constituents such as oxygen, water, and methane on exoplanets may serve as potential biosignatures (Thompson et al., 2022). For instance, the James Webb Space Telescope (JWST) has employed transit spectroscopy to characterize atmospheres of planets orbiting low-mass stars. Methane is considered a particularly promising biosignature gas. Compared to other potential biomarkers such as oxygen, isoprene, and phosphine, which are either challenging to detect or observable only in hydrogen-dominated atmospheres, methane offers relatively higher detectability due to its molecular properties. On Earth, the significant methane concentrations in the Archean atmosphere have been attributed to biological activity. In terrestrial planetary atmospheres, methane's short photochemical lifetime implies that substantial methane fluxes would be required to maintain elevated atmospheric concentrations. The photochemical lifetime of methane on Mars is approximately 300–600 years (Atreya et al., 2007). This characteristic makes methane both a sensitive indicator of potential biological activity and a challenging target for sustained detection.

The sources of methane can be biological or abiotic, such as ultraviolet degradation of organic matter, serpentinization of olivine, meteorite impacts, adsorption and desorption in the regolith, release of subsurface or subseafloor methane clathrates, weathering of basalt containing methane inclusions, and geothermal production (Webster et al., 2015).

Observations of Martian methane have been primarily ground-based and from spacecraft instruments. The Planetary Fourier Spectrometer (PFS) aboard the Mars Express (MEx) spacecraft first detected methane on Mars and suggested the possible existence of a methane reservoir in the northern polar region (Geminale et al., 2011). The Thermal Emission Spectrometer (TES) on Mars

First author: F. Y. Chen, 1437652575@qq.com
Correspondence to: R. Li, rli7@ustc.edu.cn
Received 20 MAY 2025; Accepted 20 NOV 2025.
First Published online 24 DEC 2025.

Global Surveyor (MGS) conducted global mapping of Martian methane, identifying three localized sources corresponding to Arabia Terrae—a region known for its high groundwater content—as well as the two major volcanic regions, Tharsis and Elysium (Fonti and Marzo, 2010). Observations using the Cryogenic High-Resolution Echelle Spectrometer (CSHELL) at NASA's Infrared Telescope Facility (IRTF) on Mauna Kea, Hawaii, detected localized methane plumes (~40 ppb), but subsequent observations found no methane, with a 3σ upper limit of 14 ppb (Mumma et al., 2009). The Echelon-Cross-Echelle Spectrograph (EXES) on the Stratospheric Observatory for Infrared Astronomy (SOFIA) provided an upper limit for the methane volume mixing ratio in the Martian atmosphere, ranging from 1 to 9 ppbv (Aoki et al., 2018). These observations suggest that methane release on Mars is localized and/or transient and that there may be rapid destruction mechanisms on the Martian surface (Lefèvre and Forget, 2009).

Partial pressure and volume mixing ratio are commonly used to quantify the relative abundance of a specific gas component in a mixture. The conversion between partial pressure of a gas (e.g., Pa) and its volume mixing ratio (e.g., ppbv) depends on temperature and pressure, as these parameters influence the molar volume of the gas. Partial pressure varies with temperature and atmospheric pressure, whereas the volume mixing ratio directly reflects the number of gas molecules per unit volume, making it more suitable for long-term or cross-regional comparisons of gas concentrations. Partial pressure is determined by the number of methane molecules, the temperature, and the atmospheric volume. In contrast, the volume mixing ratio depends on the total number of gas molecules and the number of methane molecules. For example, Mars exhibits significant seasonal variations in total atmospheric mass (or surface pressure). If the total atmospheric mass increases while the number of methane molecules remains constant, the volume mixing ratio decreases, yet the partial pressure stays unchanged. Conversely, if atmospheric temperature rises with a fixed number of methane molecules, the volume mixing ratio remains constant, while the partial pressure increases.

Interplanetary dust particles continuously deliver carbon sources to Mars, which can then be photolyzed by UV radiation to produce methane. The upper atmosphere of Mars is estimated to collect hundreds of tons of such organic carbon annually (Flynn, 1996). These interplanetary dust particles may contain polycyclic aromatic hydrocarbons, carboxylic acids, and amino acids. When exposed to UV photons in the 200–400 nm range, interplanetary organic carbon sources can generate methane (Stoker and Bullock, 1997; Keppler et al., 2012; Schuerger et al., 2012). These organic compounds may undergo photolysis on the Martian surface and/or within the atmosphere (Webster et al., 2018).

The Mars Science Laboratory (MSL) Curiosity rover has observed seasonal variations in atmospheric methane within Gale Crater (Webster et al., 2018). To date, several physical models have been proposed to explain the observed temporal patterns and amplitudes of these variations, including surface-based Arrhenius models and regolith diffusion-adsorption models (Moores et al., 2019a). To analyze the influence of environmental variables on methane partial pressure estimates and discriminate between potential methane production mechanisms, this study first examines key factors that may affect Martian methane concentrations. Model outputs are then compared with observational data, and Fuller's method is employed to reproduce, successfully, the seasonal methane cycle observed in Gale Crater.

2. Data

2.1 Curiosity Rover Observation Data

On August 6, 2012, at 05:18 UTC, the Curiosity rover landed as planned in Gale Crater (4.5°S, 137.4°E). The local mean solar time at touchdown was 15:03, with a solar longitude (L_s) of 150.7°.

2.1.1 Instruments and datasets for methane measurements on the Curiosity rover

The Tunable Laser Spectrometer (TLS) is a core component of the Sample Analysis at Mars (SAM) instrument suite aboard the Curiosity rover. The SAM-TLS determines methane concentrations by measuring precisely the absorption of laser light by methane molecules.

The Sample Analysis at Mars Tunable Laser Spectrometer (SAM-TLS) utilizes two distinct gas intake approaches for atmospheric analysis. The direct intake mode involves introducing atmospheric gases through an inlet into an evacuated sample cell, with the pressurization process to ~7 mbar taking approximately 20 minutes and yielding measurements with ~2 ppbv precision. Alternatively, the enrichment mode employs a CO_2 scrubber to first remove CO_2 and H_2O contaminants before gradually filling the sample cell to ~7 mbar over about 2 hours. This enrichment process amplifies methane concentrations by a factor of 25 ± 4, consequently achieving superior measurement precision. All enrichment mode measurements are below 0.7 ppbv, making this method particularly suitable for investigating background methane levels and their seasonal variations in the Martian atmosphere (Webster et al., 2018).

Methane plumes on Mars are typically sporadic and localized phenomena whose signatures are significantly affected by environmental variables such as wind speed and pressure fluctuations, potentially masking the true methane production mechanisms. Due to differences in measurement sensitivity, direct sampling methods are employed for plume detection while enrichment techniques are required for background concentration measurements. For these reasons, this study utilizes in-situ measurement data through the SAM-TLS enrichment mode. Over a five-year observational period in Gale Crater, SAM-TLS conducted ten separate enrichment-mode measurement campaigns. The results demonstrate a mean background methane level of 0.41 ± 0.16 ppbv (95% confidence interval) and reveal significant seasonal variations in methane concentration (Webster et al., 2018). This dataset provides robust constraints on Mars's atmospheric methane characteristics by minimizing interference from transient plume events and environmental noise.

2.1.2 Instrumentation and datasets for environmental measurements by the Curiosity rover

The Rover Environmental Monitoring Station (REMS) aboard the Curiosity rover conducts in situ near-surface measurements of

Martian atmospheric and surface parameters, including air/ground temperatures, atmospheric pressure, wind speed/direction, relative humidity, and UV radiation flux, enabling analysis of seasonal variations (Gómez-Elvira et al., 2012). REMS operates on an hourly cycle, collecting 5-minute measurements at 1 Hz sampling rate. During the first two Martian years, REMS observed nearly identical seasonal patterns in ground temperature variations. The model surface temperatures were obtained by calculating the average surface temperature for each solar longitude over a two-year period. Similarly, the reference atmospheric pressure profile was obtained by averaging the first two Martian years of REMS pressure measurements. Pressure data from Barocap 1 of Oscillator 2 shows an absolute accuracy of 3 Pa (Haberle et al., 2018). Air temperature measurements have 0.1 K resolution with ±5 K accuracy. Data from Mars Year 34 were excluded due to that year's prolonged global dust storm event. The annual pressure exhibits a bimodal pattern, primarily controlled by the Martian annual pressure cycle, atmospheric circulation, temperature variations, and dust storm activity. The Martian annual pressure cycle serves as the dominant controlling factor, primarily driven by seasonal condensation and sublimation of carbon dioxide in the Martian polar ice caps (Haberle and Kahre, 2010; Haberle et al., 2018; Thomas et al., 2025).

The Rover Environmental Monitoring Station (REMS) measures ultraviolet (UV) radiation flux across six spectral bands (UVABC: 210–360 nm; UVC: 215–277 nm; UVB: 270–320 nm; UVA: 315–370 nm; UVD: 230–298 nm; and UVE: 311–343 nm), with data stored in the REMS/UVS flux dataset. Initial measurements suffered from significant uncertainties caused by dust accumulation on sensors and imperfect calibration functions. To address these issues, NASA developed an improved correction algorithm that generated the UVRDR product (Vicente-Retortillo et al., 2020), which effectively corrects for both sensor dust contamination and calibration function inaccuracies. The final UVRDR product achieves a resolution better than 0.5% of the maximum measurable irradiance and an accuracy exceeding 5% of the maximum measurable irradiance. These calibrated data are archived in NASA's Planetary Data System (PDS) at https://atmos.nmsu.edu/PDS/data/mslrem_1001/DATA_UV_CORRECTED/.

2.2 Solar Ultraviolet Insolation Incident on the Martian Surface and Absorbed by the Martian Atmosphere

If carbon-bearing organic materials exist on the Martian surface, they may undergo photolysis by the incident surface UV insolation. Methane produced through this mechanism is expected to exhibit a strong correlation with the surface UV insolation. Similarly, if carbon-containing organics are present in Martian atmospheric dust, intense ultraviolet insolation could induce their photolysis, generating methane (Webster et al., 2018). Methane formed via this pathway would be expected to correlate strongly with the UV insolation absorbed by the Martian atmosphere, which is approximately equal to the difference between the top-of-atmosphere (TOA) UV insolation and the surface-reaching UV insolation. Thus, solar ultraviolet insolation represents a critical parameter governing methane concentrations in the Martian atmosphere. This necessitates concurrent measurements of both TOA and surface-level solar UV insolation on Mars. The photon energy in the UVC band is higher than that in the UVA and UVB bands. Thus this study focuses specifically on UVC insolation.

Our UVC source is the corrected flux data from the REMS/UVS UVC channel (220–280 nm). The original Mars surface REMS/UVS measurements suffered from poor accuracy due to dust deposition on sensors and inadequate calibration functions. Previous studies therefore estimated surface UV radiation through atmospheric radiative transfer modeling, using dust radiative properties derived from REMS photodiode output current products (TELRDR) and Mastcam-measured atmospheric opacity values (Vicente-Retortillo et al., 2017). This approach was necessary because atmospheric dust radiative properties—primarily single-scattering albedo and scattering phase function—are determined by dust particle refractive indices, shapes, and size distributions. Currently, both dust deposition corrections and angular response calibrations have been applied to the REMS UV flux data, which quantifies the ultraviolet radiation reaching the Martian surface.

Simultaneously, we utilized solar ultraviolet spectral irradiance data at 1 AU measured by NASA's Solar Radiation and Climate Experiment (SORCE) (Rottman, 2005) to derive top-of-atmosphere incident fluxes at Mars. SORCE, launched in January 2003 and operational until February 25, 2020, provided solar spectral irradiance measurements spanning 1 nm to 2000 nm, with daily temporal resolution in its data products.

The TOA UV flux is characterized by angular integration of top-of-atmosphere UV irradiance incident at the latitude of Gale Crater across all spatial orientations. The Martian top-of-atmosphere incident flux was first calculated as described in Equations (1)–(4) (Delgado-Bonal et al., 2016).

$$I_\lambda = I_{\lambda,0} \cdot \frac{1}{r_{\mathrm{Mars}}^2}, \tag{1}$$

where $I_{\lambda,0}$ represents the solar spectral irradiance at 1 AU observed from the SORCE database, r_{Mars} denotes the instantaneous Sun–Mars distance in astronomical units (AU), and I_λ represents the TOA radiation at Martian normal incidence. The radiometer band is denoted by λ.

The TOA radiation flux at a specific Martian location is calculated as:

$$I_{\theta,\lambda} = I_\lambda \cdot \cos(\theta), \tag{2}$$

where θ denotes the instantaneous solar zenith angle.

Assuming γ represents the solar declination, e denotes the obliquity of the ecliptic, L_s is the solar longitude, Φ represents latitude, and h stands for the solar hour angle. The calculation proceeds as follows:

$$\cos(\theta) = \sin(\Phi)\sin(\gamma) + \cos(\Phi)\cos(\gamma)\cos(h), \tag{3}$$

$$\gamma = \arcsin(\sin(e) \cdot \sin(L_s)). \tag{4}$$

Surface UV incidence on Mars refers to the angular-integrated UV irradiance incident on the Martian surface across all spatial orientations. Due to weather conditions and observational geometry, multiple invalid measurements occur during daily observations. Temporal gaps in the data may introduce errors in subsequent integration processes. To address missing values, this study

employs adjacent-time SORCE TOA UVC calculations ($I_{\Phi,\lambda}$) and valid REMS/UVS UVC measurements ($I_{\Phi,\lambda,\mathrm{sur}}$) to compute atmospheric opacity (τ) using Equation (5). The τ values calculated from adjacent time points are interpolated to obtain τ for the missing time periods. These interpolated τ values are then substituted into Equation (5) to calculate $I_{\Phi,\lambda,\mathrm{sur}}$ for the missing time periods.

$$I_{\Phi,\lambda,\mathrm{sur}} = I_{\Phi,\lambda} \cdot \mathrm{e}^{\frac{-\tau}{\cos(\theta)}}, \tag{5}$$

where $I_{\Phi,\lambda,\mathrm{sur}}$ represents the surface-reaching ultraviolet radiation flux and τ denotes atmospheric opacity.

By integrating the surface-incident radiation flux over an entire Martian day (sol), we obtain the daily UVC insolation, as shown in Figure 1.

Results indicate that during aphelion season (L_s = 0°–180°), atmospheric opacity (τ) is relatively low, with the annual minimum occurring at L_s ~125°. In contrast, τ increases during perihelion season (L_s = 180°–360°). Enhanced dust activity during perihelion is the most likely explanation of the two observed relative maxima centered at L_s = 210°–270° and L_s = 310°–350°, respectively; the local τ minimum at L_s ~300° corresponds to a period of quiescent dust activity between these two dust storm episodes, corresponding to the dust storms in seasons A and C (Kass et al., 2016). These findings are consistent with prior studies (Vicente-Retortillo et al., 2017).

3. Modeling the Relationship Between Surface Methane Concentration and Environmental Variables

Multiple methods have been employed to identify and quantify relationships between variables for pattern analysis. For instance, correlation coefficients, least squares regression analysis, and the maximal information compression index are widely used to assess inter-variable correlations. On Earth, correlation coefficients have frequently been applied to analyze the influence of environmental variables (e.g., precipitation and temperature) on methane concentrations (Peng SS et al., 2022). Therefore, this study utilizes correlation coefficients to evaluate the relationship between surface methane concentrations and environmental variables on Mars.

Webster et al. (2018) employed chi-square tests to conduct extensive correlation analyses between measured methane concentrations and environmental variables on Mars (e.g., atmospheric pressure, temperature, and UV flux). They concluded that a simple linear relationship between methane concentration and these environmental variables is unlikely.

Correlation coefficients measure the consistency of variation trends, while reduced chi-squared statistics evaluate deviations between linearly modeled results and observed data. If the relationship between methane concentration and an environmental variable is nonlinear, the correlation coefficient might suggest a strong association, whereas the chi-square test of the same variable's influence would suggest that a linear relationship is unlikely to exist. Aware of the limitations of these two approaches, our study employs both, calculating correlation coefficients as well as employing chi-square tests.

Furthermore, reproducing the seasonal cycle of methane concentrations through physical models can provide deeper insights into potential methane production mechanisms. Below, we introduce, in sequence, five commonly used physical models for characterizing atmospheric CH_4 concentrations on Mars (Moores et al., 2019a). The origin of methane in Gale Crater remains uncertain; this study conducts a comparative analysis of several plausible hypotheses to assess the validity of each.

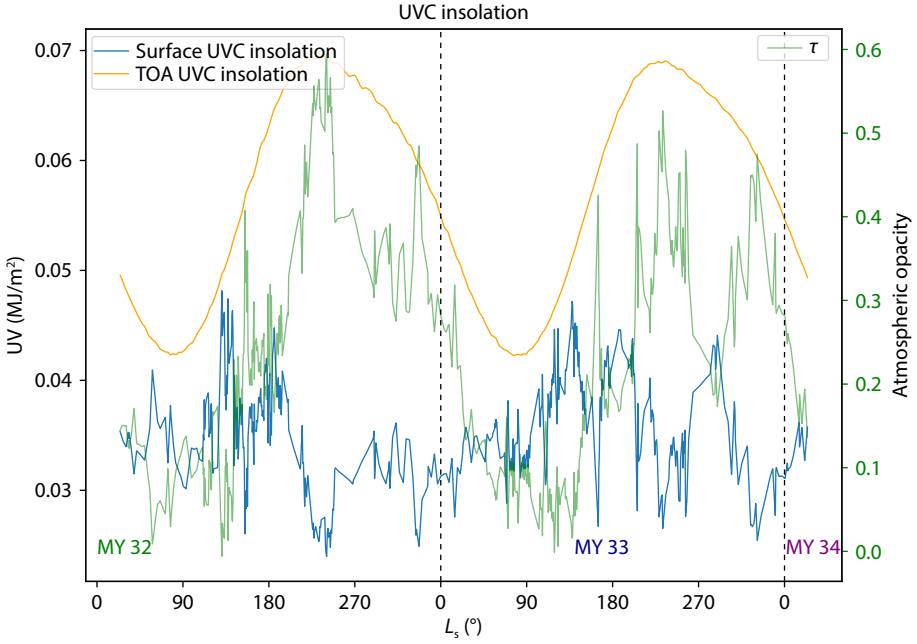

Figure 1. Diurnally integrated TOA UVC insolation (orange line) and surface UVC insolation (blue line) over a full Martian sol. The atmospheric opacity (τ) is shown in green. MY denotes Mars Year.

3.1 Arrhenius Model

The fundamental physical process of the Arrhenius model is thermal activation. For a reaction to occur, an energy barrier (i.e., the activation energy, E_a) must be overcome. Webster et al. (2018) adopted an E_a value of 32 kJ/mol for methane desorption. Active adsorption sites exist on pore walls, where gas molecules can adsorb and subsequently desorb via thermal activation, overcoming the energy barrier—a process whose temperature dependence follows the Arrhenius equation. The Arrhenius model thus simulates seasonal variations in Martian methane concentration by assuming that they are caused primarily by methane exchange between the Martian surface and the planet's atmosphere.

In the Arrhenius model, methane emissions from the regolith surface are dependent solely on temperature, as expressed in Equation (6).

$$p = a \cdot T_{\mathrm{sur}}^{0.5} \cdot \mathrm{e}^{\frac{-32\times10^3}{RT_{\mathrm{sur}}}} + b, \tag{6}$$

where p denotes the partial pressure of methane (in ppbv), T represents ground temperature, and R is the universal gas constant. The parameter a corresponds to the atmospheric layer thickness (units: m) with sufficient gas exchange at the regolith surface, while b represents Mars' intrinsic methane background concentration. Through least-squares fitting, we obtain $a = 3\times10^4$ and $b = 0.1$.

3.2 Knudsen Diffusion Model

Knudsen diffusion refers to a transport phenomenon that occurs under conditions of either extremely low pressure or within confined pores (where the pore diameter is smaller than the mean free path of gas molecules). In this regime, the frequency of gas molecule collisions with pore walls significantly exceeds intermolecular collisions. Consequently, mass transfer is dominated by molecule-wall interactions rather than intermolecular collisions.

The transport of gases through adsorption and desorption in regolith pores can be described by Knudsen diffusion:

$$D_{\mathrm{kn}} = \frac{d}{3}\sqrt{\frac{8RT}{\pi M_{\mathrm{CH_4}}}}, \tag{7}$$

where d represents the pore diameter in subsurface regolith ($d = 1\times10^{-5}$ m), $M_{\mathrm{CH_4}}$ denotes the molecular weight of methane ($M_{\mathrm{CH_4}} = 0.016$ kg mol^{-1}), and T is the regolith temperature, which varies as a function of depth below the surface.

Assuming a methane leakage source at depth, the deep subsurface methane mixing ratio is denoted as p_0 (Pa). Since p_0 exhibits minimal seasonal variation, it is treated as a constant. The concentration difference induced by the regolith sub-column can be expressed as:

$$\Delta p = \frac{F\times R\times T\times H}{DM_{\mathrm{CH_4}}}, \tag{8}$$

where D is the diffusion coefficient. F represents the methane flux from the subsurface source. An active, continuous, steady-state deep source of methane is assumed. Consequently, the methane flux F would exhibit minimal seasonal variation and is therefore treated as a constant (kg m^{-2} s^{-1}). H is the diffusion distance (m). Along the subsurface temperature profile, we sequentially calculate Δp (Pa) to derive the surface methane concentration. Finally, p_0 and F are determined through least-squares fitting.

3.3 Regolith Adsorption-Desorption Model

Moores et al. (2019a) employed a one-dimensional numerical model incorporating both subsurface emission sources and adsorption–diffusion processes. This model describes how gaseous diffusion couples dynamically with surface adsorption–desorption kinetics during gas transport through porous media (e.g., Martian regolith), an interaction that manifests ultimately as variations in effective diffusivity. When diffusing gas molecules collide with pore walls, they may become adsorbed, requiring a finite desorption time before continuing their diffusion path. This process introduces a temporal delay compared to pure Knudsen diffusion.

The model accounts for the regolith's adsorption capacity (φ) and the influence of adsorption isotherm slope on gas diffusivity, yielding an effective diffusion coefficient (D_{eff}).

$$\frac{\partial p}{\partial t} = D_{\mathrm{kn}}\frac{\partial^2 p}{\partial x^2} - \varphi\frac{\partial \delta}{\partial p} = D_{\mathrm{eff}}\frac{\partial^2 p}{\partial x^2}, \tag{9}$$

$$D_{\mathrm{eff}} = \frac{D_{\mathrm{kn}}}{1+\varphi\dfrac{\partial \delta}{\partial p}}, \tag{10}$$

$$\varphi = R_{\mathrm{CH_4}} T \rho_{\mathrm{reg}} A_s m_{\mathrm{ML}}, \tag{11}$$

where φ represents the regolith's adsorption capacity (unitless), δ denotes surface coverage (unitless), $R_{\mathrm{CH_4}}$ is the specific gas constant for methane ($R_{\mathrm{CH_4}} = 518.2$ J kg^{-1} K^{-1}), ρ_{reg} indicates the bulk density of regolith ($\rho_{\mathrm{reg}} = 1300$ kg m^{-3}), A_s represents the specific surface area of regolith ($A_s = 3\times10^4$ m^2 kg^{-1}), and m_{ML} is the mass per unit area of a single adsorption monolayer ($m_{\mathrm{ML}}=1.38\times10^{-7}$ kg m^{-2}). The larger the φ value, the greater the number of molecules that can be adsorbed per unit area. The steeper the slope of the adsorption isotherm ($\frac{\partial \delta}{\partial p}$), the higher the probability of gas molecules being adsorbed after diffusing to pore walls. The transient adsorption–desorption kinetics are described by:

$$\frac{\partial \delta}{\partial t} = k_a p\left(\delta_{\mathrm{eq}} - \delta\right) - k_d\delta, \tag{12}$$

where, δ_{eq} represents the surface coverage at adsorption equilibrium ($t\rightarrow\infty$). k_d denotes the desorption rate constant, and k_a is the adsorption rate constant (units: s^{-1}).

At equilibrium ($\frac{\partial \delta}{\partial t} = 0$), the following relation holds:

$$\delta_{\mathrm{eq}} = \frac{k_{\mathrm{eq}}p_{\mathrm{eq}}}{1+k_{\mathrm{eq}}p_{\mathrm{eq}}}, \tag{13}$$

where, p_{eq}(in ppbv) denotes the equilibrium methane concentration after adsorption. k_{eq} represents the net equilibrium rate constant between adsorption and desorption processes. The solution is derived using the integrating factor method:

$$\delta(t) = \frac{k_a p_{\mathrm{eq}} p}{k_d + k_a p}\left(1 - \mathrm{e}^{-(k_a p + k_d)t}\right), \tag{14}$$

The derivative is:

$$\frac{\partial \delta}{\partial p} = \frac{k_{eq}}{\left(1 + k_{eq}p\right)^2}\left[1 + \left(k_{eq}pk_d t\left(1 + k_{eq}p\right) - 1\right)\mathrm{e}^{\left(-k_d\left(1+k_{eq}p\right)t\right)}\right], \quad (15)$$

where t represents the time step governing the temporal resolution of the effective diffusion coefficient (D_{eff}). The model computes methane concentrations at intervals of one Martian sol.

Finally, substituting D_{eff} into Equation (8) yields the surface methane concentration. p_0 and F are derived via least-squares fitting.

3.4 Fuller's Formulation

Klusman et al. (2024) proposed a model combining barometric pumping and molecular diffusion (the B–P model) as a leading candidate to explain methane concentrations on the Martian surface. Moores et al. (2019b) proposed that molecular diffusion could be the dominant mechanism for gas mixing after the collapse of the nocturnal planetary boundary layer. Therefore, it may be justified to use molecular diffusion to estimate subsurface and near-surface methane concentrations.

Fuller's method is a semi-empirical formulation for predicting binary gas diffusion coefficients (Fuller et al., 1966; Poling et al., 2001). This approach can characterize gas diffusion in both atmospheric and porous media systems. For Mars, we consider a three-zone structure: deep subsurface methane sources; low-permeability zones (comprising dense salt crusts or permafrost); and near-surface high-permeability zones (fracture networks or porous sedimentary layers). In high-permeability regions, intermolecular collisions dominate diffusion kinetics; atmospheric pressure thus serves as the critical controlling factor. Under elevated pressure conditions, the number density of gas molecules increases, resulting in higher intermolecular collision frequencies, which reduce the mean free path of molecules and leads to decreased diffusion rates. Conversely, gas transport in low-permeability zones is governed primarily by diffusion dominated by molecule-wall collisions.

In this study, we adopt Fuller's method, assuming that intermolecular collisions are the main controlling process in the Martian methane observations we analyze.

In Fuller's method, the gas diffusion coefficient in the Martian atmosphere is expressed as (Klusman et al., 2024):

$$D_{air} = \frac{0.0014 \times T^{1.75}}{P} - \frac{\left(\frac{1}{M_{air}} + \frac{1}{M_{CH_4}}\right)^{\frac{1}{2}}}{\left[\left(\sum V_{air}\right)^{\frac{1}{3}} + \left(\sum V_{CH_4}\right)^{\frac{1}{3}}\right]^2}, \quad (16)$$

where P is the total atmospheric pressure (Pa), M_{air} represents the molecular weight of Martian 'air' (43.337 g mol^{-1}), and M_{CH_4} denotes methane's molecular weight (16.04 g mol^{-1}). $\sum V_{air}$ and $\sum V_{CH_4}$ are the diffusion volumes of Martian 'gas' (27.385 cm^3 mol^{-1}) and methane (25.14 cm^3 mol^{-1}), respectively.

The Millington–Quirk formula (Devitt et al., 1987) describes porosity (ε) effects on the diffusion coefficient of Martian 'air' in the top 30 m of regolith:

$$D_{sed} = \varepsilon^{\frac{4}{3}} \cdot D_{air}. \quad (17)$$

Finally, substituting D_{sed} into Equation (8) yields the surface methane concentration. p_0 and F are derived via least-squares fitting.

The upper boundary condition for regolith temperature is given by

$$T(0, t) = T_{ave} + A \cdot \sin\left(\omega t + \beta\right), \quad (18)$$

where T_{ave} is the diurnal mean temperature at 0 m depth, A represents the amplitude of the temperature wave, t denotes time, ω is the planetary rotation angular velocity, and β stands for the phase shift.

The temperature at a depth of z meters is given by (Arya, 1988)

$$(z, t) = T_{ave} + A \cdot \mathrm{e}^{-\alpha z} \cdot \sin\left(\omega t + \beta - \alpha z\right), \quad (19)$$

$$\alpha = \sqrt{\frac{\omega}{2k}}, \quad (20)$$

where k is the thermal diffusivity of the regolith (m^2 s^{-1}), and α represents the depth-dependent attenuation coefficient for both amplitude and phase. The subsurface temperature profile is calculated at 0.5 m depth intervals.

The subsurface pressure profile is computed following Arya (1988):

$$D_d = \left(\frac{2}{\omega} \cdot \frac{KP_{ave}}{\eta\varepsilon}\right)^{\frac{1}{2}}, \quad (21)$$

$$P(z) = P_{ave} + B \cdot \mathrm{e}^{\frac{-z}{D_d}} \cdot \sin\left(\omega t + \mu - \frac{z}{D_d}\right), \quad (22)$$

where K is the permeability ($K = 10^{-10}$ m^2), P_{ave} represents the mean pressure (Pa), ε denotes porosity ($\varepsilon = 0.1$), μ is the phase (dimensionless), and η indicates the viscosity of the gas phase ($\eta = 1.058 \times 10^{-5}$ Pa s).

3.5 UV-Driven Organic Photolytic Model

UV photolysis is a process that synergistically combines UV radiation and thermal effects to decompose organic matter, releasing methane. The fundamental mechanisms are (a) UV photon energy breaks chemical bonds in organic compounds, and (b) heating promotes photolytic reactions, creating a 'photo-thermal synergistic catalysis' effect that ultimately converts large organic molecules into small gas molecules, such as methane.

The methane flux produced by UV photolysis of organic matter is determined by the strength of the UV radiation flux and by the relevant *quantum efficiency* (*QE*) of the photolysis. *QE* is a function of organic carbon content, organic matter temperature, and photolytic duration. As photolytic time increases, the amount of organic matter within the UV penetration depth decreases, leading to a reduction in *QE*. Assuming the organic materials are freshly exposed, the calculated total methane represents the upper limit of methane production from organic photolysis in Gale Crater (Moores et al., 2017):

$$QE = 2.76 \times 10^{-10} F_{CH_4}\left[5.8 \times 10^{-4}\left(T - 273.15\right) + 0.126\right]\left[6.9x + 0.026\right], \quad (23)$$

where QE represents the quantum efficiency of organic carbon-to-methane conversion (mol J^{-1}), F_{CH_4} denotes the methane flux (laboratory measurements yielded F_{CH_4} = 0.145 nmol g^{-1} h^{-1}, which represents the maximum value obtained from Martian sample fitting), and x indicates the mass fraction of carbon in organic matter, taken as x = 0.0169 based on the Murchison meteorite analog sample.

$$N_{CH_4} = QE \times \text{flux}, \tag{24}$$

where flux represents the ultraviolet radiation (J m^{-2}) and N_{CH_4} denotes the total methane quantity (mol).

$$p_{CH_4} = 10^9 N_{CH_4} \frac{g_{Mars} M_{CO_2}}{p_{CO_2}}, \tag{25}$$

where p_{CH_4} denotes the partial pressure of methane (in ppbv), g_{Mars} represents Martian surface gravity (g_{Mars} = 3.724 N kg^{-1}), M_{CO_2} is the molecular weight of carbon dioxide (M_{CO_2} = 0.044 kg mol^{-1}), and p_{CO_2} stands for the surface pressure of CO_2 (p_{CO_2} = 610 N m^{-2}).

4. Results

4.1 Correlation Analysis Between Surface Environmental Factors and Methane Concentration

To analyze relationships between methane concentrations and the following Martian surface environmental variables, we calculated correlation coefficients between methane concentrations and as shown in Figure 2, surface pressure, ground temperature, surface UVC insolation, and UVC insolation absorbed by the atmosphere.

The results indicate that the methane mixing ratio shows no significant correlation with ground temperature, UVC insolation absorbed by the atmosphere, or surface UVC insolation, but does exhibit a significant negative correlation with surface pressure. Surface pressure may therefore be a key factor influencing methane partial pressure. We note that this relationship may have emerged because the rover's continuous ascent has led to progressively decreasing "surface" pressure over the time the rover has been collecting data. This implies that models neglecting pressure effects will exhibit progressively increasing errors over time.

4.2 Model Accuracy Validation

We now compare measured values to the surface methane concentrations simulated by the aforementioned five models. The results are presented in Figures 3 and 4.

Fuller's method shows the smallest deviation from the measured values, probably because it accounts for the diffusion of shallow subsurface methane gas driven by seasonal variations in atmo-

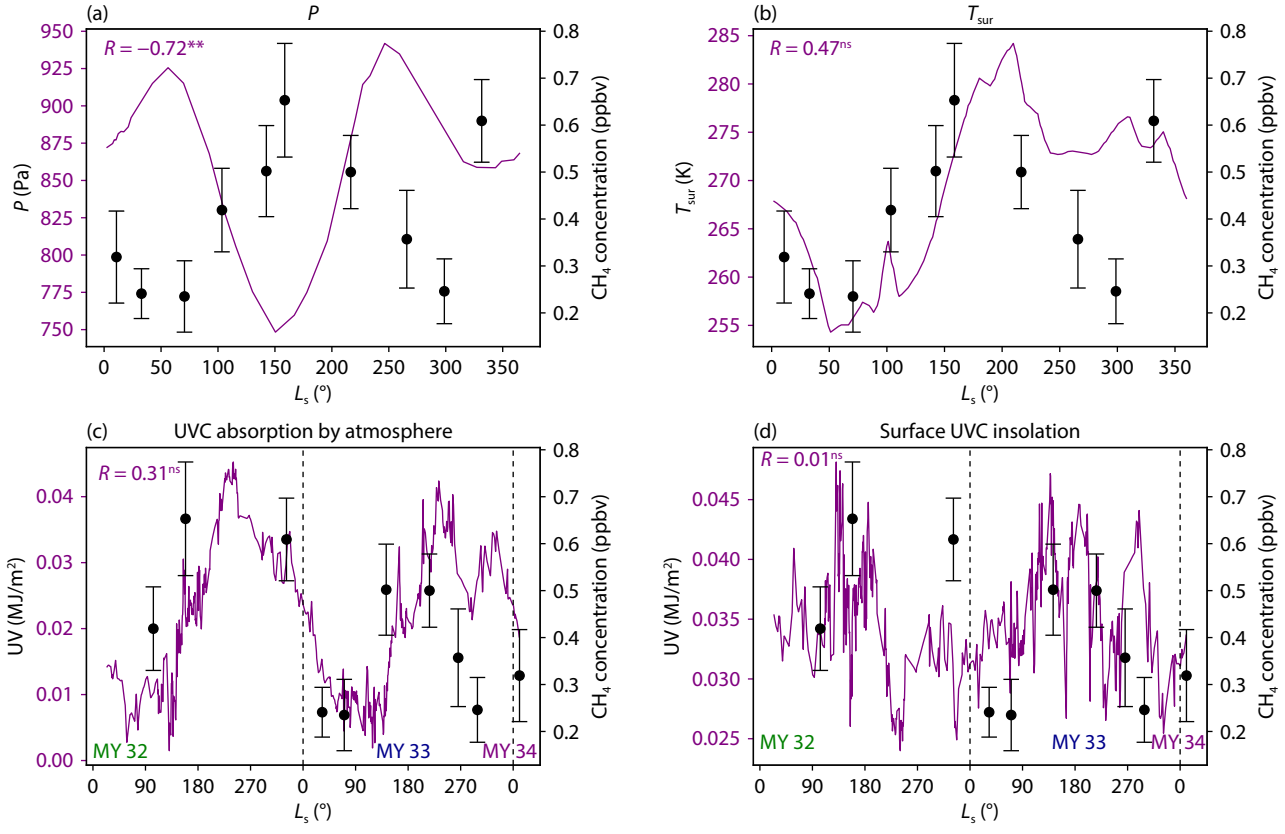

Figure 2. Time series curves of (a) surface pressure, (b) ground temperature, (c) UVC insolation absorbed by the atmosphere, and (d) surface UVC insolation near Gale Crater. Black dots represent actual SAM-TLS measurements of methane, with error bars indicating ±1 s.e.m. (standard error). The correlation coefficient between methane concentration and each environmental factor is labeled in the upper left corner of each panel (** indicates $P < 0.05$, ns indicates not significant). Surface pressure and ground temperature were obtained by averaging REMS measurements from the first two years. MY denotes *Mars Year*.

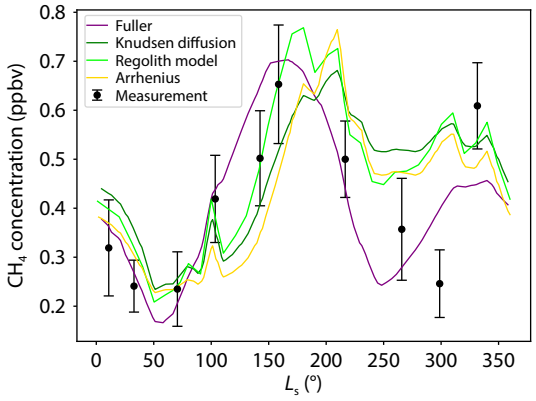

Figure 3. Methane concentration time series in Gale Crater estimated by these models: Fuller's method, Knudsen diffusion, regolith diffusion-adsorption, and Arrhenius. Black dots represent actual SAM-TLS measurements of methane, with error bars indicating ±1 s.e.m. (standard error).

spheric pressure and temperature.

In the Arrhenius model, see Equation (6), the pre-exponential factor represents the thickness of the atmosphere that is exchanging methane with the regolith surface. Based on fitting results, this value reaches 10^4, a magnitude suggesting that the Arrhenius model unrealistically assumes complete methane exchange between the regolith surface and all tens of kilometers of atmosphere. Equation (6) also includes an offset term representing Mars' inherent methane background concentration. Again according to fitting results, the Arrhenius model needs to assume a Martian methane background concentration of 0.1 ppbv to fit its output to actual observations, whereas ExoMars Trace Gas Orbiter observations indicate an actual methane upper limit of approximately 0.05 ppbv (Korablev et al., 2019). These findings suggest the Arrhenius model may be unrealistic.

In the regolith diffusion-adsorption model, see Equation (15), sustained increases or decreases in daily temperature amplify phase lag, particularly during L_s = 100–200°, a feature that is not accounted for in either the Knudsen diffusion model or the Arrhenius model. Phase lag refers to the time delay between temperature changes and gas adsorption–desorption responses. Before methane molecules can be released, they must first occupy adsorption sites in the regolith; this sequence complicates the methane concentration's response to temperature variations. The regolith diffusion–adsorption model simulates phase lag by introducing time t in Equation (15). The one-dimensional numerical model of adsorption and diffusion is used to describe how gas phase diffusion is dynamically coupled with surface adsorption desorption kinetics during gas transport in porous media such as Martian weathered layers, ultimately resulting in a change in the effective diffusion rate. When gas diffusion collides with pore walls, it may be adsorbed by surface active sites where it waits for desorption before continuing diffusion, delaying diffusion time compared to simple Knudsen diffusion. When the transient diffusion coefficient asymptotically approaches a constant value (denoted as the steady-state diffusion coefficient) as time extends to infinity, temperature becomes the sole determining factor. During the non-steady-state period, a measurable discrepancy persists between the transient and the steady-state diffusion coefficients. Sustained temperature trends over short timescales induce cumulative divergence between these coefficients, consequently intensifying the phase retardation effect. When temperature rises, methane concentration initially increases rapidly before gradually approaching equilibrium (steady-state). The time required to reach approximately 90% of the pressure difference is called the equilibration time. A time step of one Martian sol may be insufficient for the regolith to reach steady-state, requiring

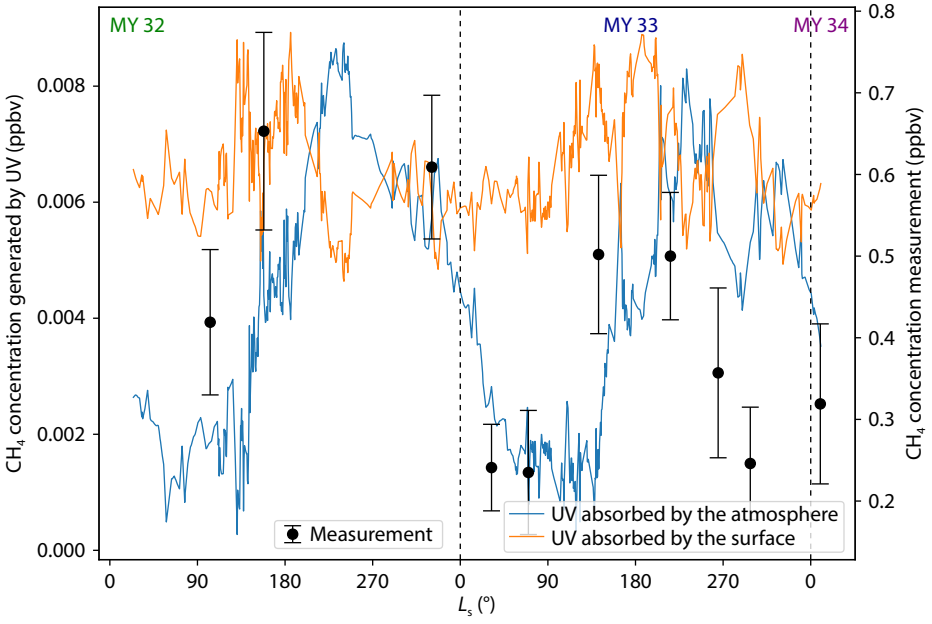

Figure 4. Methane concentrations produced through (a) atmospheric UVC insolation-absorption-driven organic photolysis (blue line) and (b) surface UVC insolation-induced organic photolysis (orange line). Black data points indicate SAM–TLS measured methane concentrations, with error bars representing ±1 s.e.m. (standard error).

Equation (15) to calculate the actual diffusion rate in non-steady-state regolith. In contrast, both the Knudsen diffusion model and Arrhenius model assume the regolith is always in steady-state, ignoring equilibration time.

However, in the Fuller method, pressure and temperature jointly influence the rate of methane transport through the subsurface. Fuller's method assumes that the frequency of collisions between gas molecules and pore walls is significantly lower than the frequency of mutual collisions among gas molecules. Consequently, the contribution to the overall transport process of adsorption–desorption events and associated time lags is negligible.

Figure 3 demonstrates that the primary discrepancy between Fuller's method and the other models occurs between L_s = 240° and L_s = 320°. This divergence may result from the abrupt increase in atmospheric pressure driven by the annual carbon dioxide sublimation cycle. During this period, while temperature shows no significant decrease, atmospheric pressure reaches its seasonal maximum. Consequently, Fuller's method, sensitive to both pressure and temperature, predicts a sharp decline in methane concentration; the other models do not.

Although pressure gradients serve as one of the primary drivers of gas transport through porous regolith and sedimentary rocks, the model of Moores et al. (2019a) does not account for atmospheric pressure effects on methane concentration. Furthermore, while their model is applicable to deep subsurface geological formations with low permeability, it cannot be extended to high-permeability shallow regolith where methane diffusion is governed predominantly by intermolecular collisions.

Fuller's method, however, can accurately describe this collision-dominated diffusion regime while simultaneously incorporating both pressure and temperature effects on gas transport. Its superior accuracy follow from its strong physical basis, unlike models that adjust arbitrary fitting coefficients. Fuller's method captures the variation of methane diffusivity with the Martian changes of seasons—observable temporal variations that are large.

Carbon-bearing organic compounds may exist either in the Martian atmosphere or on the surface, where they undergo photolysis by ultraviolet radiation—either absorbed by the atmosphere or reaching the surface—to produce methane. Assuming contributions from freshly exposed organics, our UV-driven organic photolytic model simulates the upper limits of methane production from both surface-incident UVC (observed values) and atmospherically absorbed UVC (calculated values), as shown in Figure 4. Even if the SAM–TLS measurements are assumed to represent methane concentrations throughout the entire diurnal cycle in Gale Crater, the simulated values remain significantly lower than the measured concentrations.

Furthermore, previous studies suggest that, during daytime in Gale, when the planetary boundary layer (PBL) is fully developed, the eddy diffusion coefficient may reach values on the order of thousands of $m^2\ s^{-1}$—far exceeding molecular diffusivity ($10^{-3}\ m^2\ s^{-1}$) (Taylor et al., 2007; Pathak et al., 2008; Moores et al., 2019b). This intense turbulent mixing would rapidly disperse UV-generated methane to other regions. At night, radiative cooling creates temperature inversions and triggers PBL collapse (Guzewich et al., 2017). Dynamical models indicate that nocturnal inversion layers and convergent downslope winds may suppress turbulent mixing, while daytime turbulence would be expected to enhance vertical mixing and advect methane out of the crater region, potentially diluting concentrations (Webster et al., 2021).

Curiosity's sampling occurs after PBL collapse. If this mechanism is correct, the residual methane produced from UVC photolysis of organics following PBL collapse remains unquantified. However, it is expected to constitute only a minor fraction of the measured values.

Root mean square error (RMSE) and goodness-of-fit (R^2) were calculated between model results and measured values, as shown in Table 1. An outlier at L_s = 331°, potentially representing a methane plume, was excluded from the analysis as it significantly reduced the overall fitting quality (Moores et al., 2019b).

The Fuller method demonstrates superior performance with a goodness-of-fit (R^2) of 0.84, significantly outperforming other models, probably because of its incorporation of pressure as an independent variable. Fuller's method also achieves the smallest root mean square error (RMSE = 0.005), followed by the regolith diffusion–adsorption model's 0.019.

The UV-driven organic photolytic model shows the poorest performance, strongly suggesting that photolysis is unlikely to be the dominant methane production mechanism in Gale Crater.

5. Discussion and Conclusions

The origin of methane in Gale Crater on Mars thus remains an unanswered question, suggesting that other explanations be investigated in greater detail. One alternative mainstream hypothesis is that methane might originate from other regions and be transported to the Curiosity rover site by horizontal wind fields (Giuranna et al., 2019; Luo Y et al., 2021).

Methane concentrations measured by the Curiosity rover are reported as volume mixing ratios. The total atmospheric mass (or surface pressure) of Mars exhibits significant seasonal variations, with diurnally averaged pressure changes reaching up to ~200 Pa (Haberle et al., 2018). Pressure gradients are one of the driving

Table 1. RMSE and R^2.

	Fuller's method	Arrhenius model	Knudsen diffusion model	Regolith adsorption–desorption model	Atmospheric UVC insolation-driven organic photolytic model	Surface UVC insolation-driven organic photolytic model
RMSE	0.005	0.031	0.030	0.019	0.165	0.162
R^2	0.84	0.10	0.13	0.47	0.03	0.13

forces of gas transport into or out of porous regolith/sedimentary rocks. Although Moores et al. (2019a) successfully reproduced the methane concentrations in Gale Crater using a 1D numerical model that accounts for subsurface leakage sources, adsorption, and diffusion, their model did not consider the influence of atmospheric pressure on methane concentrations. Furthermore, the model of Moores et al. (2019a) is most applicable to deep subsurface geological regions with low permeability but not to high-permeability shallow regolith, where methane diffusion is likely dominated by intermolecular collisions. In contrast, Fuller's method can describe gas diffusion dominated by intermolecular collisions while simultaneously accounting for the effects of both pressure and temperature on gas diffusion.

Correlation analysis reveals a strong negative relationship between methane concentrations and surface atmospheric pressure on Mars, while surface temperature, another potentially important influencing factor, shows no significant correlation. We suggest that replacing correlation coefficients with causality metrics may provide a better analytical approach. Correlation coefficients are useful primarily to assess linear relationships. In contrast, certain causality metrics, such as Klimontovich information flow, provide better interpretation when multifactorial coupling functions include nonlinear relationships.

This study compared simulated results from five commonly used Martian surface CH_4 models with in-situ rover measurements, revealing that Fuller's model—which incorporates atmospheric pressure as a key factor—shows the best agreement with observational data. Correlation analysis between multiple environmental variables and methane concentrations demonstrated a strong negative correlation between atmospheric pressure and methane levels. The pressure effect, driven by seasonal variations in atmospheric pressure, may represent the dominant mechanism controlling methane variability in Gale Crater. Since 2014, as Curiosity has been ascending the crater's slopes, the increasing elevation at which measurements have been made is correlated with a continuous decrease in surface atmospheric pressure. Failure to account for this pressure effect in methane concentration modeling may introduce significant errors.

During the methane concentration measurement period, the seasonal variation in Martian surface pressure (>20%) results primarily from the condensation/sublimation of CO_2 in the planet's polar regions (Thomas et al., 2025). Atmospheric pressure decreases approximately exponentially with altitude. Given that Mount Sharp has an elevation of ~5.5 km, the atmospheric pressure at its summit is about 60% of that at the crater floor. During methane observation periods, Curiosity rover ascended to the foothills of Mount Sharp, with a cumulative vertical climb of ~300 m, resulting in an estimated ~3% pressure decrease relative to the crater floor. Therefore, the currently measured atmospheric pressure variations are predominantly driven by seasonal CO_2 cycling in the polar regions. While altitude-induced pressure changes (and their consequent limitations on methane concentration) are localized and non-seasonal, they may become significant factors in future observations.

If methane sources are located underground, methane diffusion would likely be constrained by atmospheric pressure. Given Mars' low methane concentrations, priority should be given to detecting methane during seasons with higher surface temperatures and lower atmospheric pressure, as these conditions may optimize the identification of potential subsurface methane sources. For a subsurface methane seepage source with constant flux, decreased atmospheric pressure may lead to elevated methane concentrations.

The upper limit for methane production from UVC photolysis of organics is on the order of 1 pptv. This contrasts with the ExoMars Trace Gas Orbiter's (TGO) global methane upper limit of 50 pptv and Curiosity's measured background methane levels of <700 pptv. Even if active UVC photolysis of organics occurs in Gale Crater, the resulting methane would represent only a minor contribution to the observed background levels. Microseepage may be the primary methane source in Gale Crater. Additionally, active ultraviolet photolysis of organic matter within the UVA and UVB wavelength ranges remains a possibility. However, the types and abundance of organic materials on the Martian surface are still not well understood. UVC photons possess the highest energy and can directly break more chemical bonds in organic compounds, making them likely to be more efficient than UVA and UVB in initiating photolytic reactions.

This study calculated upper limits for methane production through UVC photolysis of organics; we find that these upper limits appear to be substantially lower than measured values. Furthermore, most UV-driven photolysis occurs prior to times of planetary boundary layer collapse, with intense turbulent mixing during this period further reducing any residual methane concentrations.

Acknowledgments

The authors declare that they have no known competing financial interests or conflicts of interest. This work was supported by the National Natural Science Foundation of China NSFC (Grant No. 42330602, 42275139), the National Key Research and Development Program of China (Grant No. 2024YFF0809401), the Anhui Provincial Natural Science Foundation (Grant No. 2208085UQ02), Innovation Center for Fengyun Meteorological Satellite Special Project (Grant No. FY-APP-ZX-2022.0211), and the Joint Laboratory of Fengyun Remote Sensing.

References

Aoki, S., Richter, M. J., DeWitt, C., Boogert, A., Encrenaz, T., Sagawa, H., Nakagawa, H., Vandaele, A. C., Giuranna, M., … Kasaba, Y. (2018). Stringent upper limit of CH_4 on Mars based on SOFIA/EXES observations. *Astron. Astrophys.*, *610*, A78. https://doi.org/10.1051/0004-6361/201730903

Arya, S. P. (1988). *Introduction to Micrometeorology*. San Diego: Academic Press.

Atreya, S. K., Mahaffy, P. R., and Wong, A. S. (2007). Methane and related trace species on Mars: Origin, loss, implications for life, and habitability. *Planet. Space Sci.*, *55*(3), 358–369. https://doi.org/10.1016/j.pss.2006.02.005

Delgado-Bonal, A., Zorzano, M. P., and Martín-Torres, F. J. (2016). Martian Top of the Atmosphere 10–420 nm spectral irradiance database and forecast for solar cycle 24. *Solar Energy, 134*, 228–235. https://doi.org/10.1016/j.solener.2016.05.004

Devitt, D. A., Evans, R. B., Jury, W. A., Starks, T. H., and van Ee, J. J. (1987). Soil Gas Sensing for Detection and Mapping of Volatile Constituents. National Water Well Assoc, Dublin, Ohio, 270.

Flynn, G. J. (1996). The delivery of organic matter from asteroids and comets to the early surface of Mars. *Earth Moon Planets*, *72*(1), 469–474. https://doi.org/10.1007/BF00117551

Fonti, S., and Marzo, G. A. (2010). Mapping the methane on Mars. *Astron. Astrophys.*, *512*, A51. https://doi.org/10.1051/0004-6361/200913178

Fuller, E. N., Schettler, P. D., and Giddings, J. C. (1966). New method for prediction of binary gas-phase diffusion coefficients. *Ind. Eng. Chem.*, *58*(5), 18–27. https://doi.org/10.1021/ie50677a007

Geminale, A., Formisano, V., and Sindoni, G. (2011). Mapping methane in Martian atmosphere with PFS-MEX data. *Planet. Space Sci.*, *59*(2–3), 137–148. https://doi.org/10.1016/j.pss.2010.07.011

Giuranna, M., Viscardy, S., Daerden, F., Neary, L., Etiope, G., Oehler, D., Formisano, V., Aronica, A., Wolkenberg, P., … Amoroso, M. (2019). Independent confirmation of a methane spike on Mars and a source region east of Gale Crater. *Nat. Geosci.*, *12*(5), 326–332. https://doi.org/10.1038/s41561-019-0331-9

Gómez-Elvira, J., Armiens, C., Castañer, L., Domínguez, M., Genzer, M., Gómez, F., Haberle, R., Harri, A. M., Jiménez, V., … Martín-Torres, J. (2012). REMS: The environmental sensor suite for the mars science laboratory rover. *Space Sci. Rev.*, *170*(1), 583–640. https://doi.org/10.1007/s11214-012-9921-1

Guzewich, S. D., Newman, C. E., Smith, M. D., Moores, J. E., Smith, C. L., Moore, C., Richardson, M. I., Kass, D., Kleinböhl, A., … Battalio, M. (2017). The vertical dust profile over Gale Crater, Mars. *J. Geophys. Res.: Planets*, *122*(12), 2779–2792. https://doi.org/10.1002/2017JE005420

Haberle, R. M., and Kahre, M. A. (2010). Detecting secular climate change on Mars. *Mars*, *5*, 68–75. https://doi.org/10.1555/mars.2010.0003

Haberle, R. M., de la Torre Juárez, M., Kahre, M. A., Kass, D. M., Barnes, J. R., Hollingsworth, J. L., Harri, A. M., and Kahanpää, H. (2018). Detection of Northern Hemisphere transient eddies at Gale Crater Mars. *Icarus*, *307*, 150–160. https://doi.org/10.1016/j.icarus.2018.02.013

Kass, D. M., Kleinböhl, A., McCleese, D. J., Schofield, J. T., and Smith, M. D. (2016). Interannual similarity in the Martian atmosphere during the dust storm season. *Geophys. Res. Lett.*, *43*(12), 6111–6118. https://doi.org/10.1002/2016GL068978

Keppler, F., Vigano, I., McLeod, A., Ott, U., Früchtl, M., and Rockmann, T. (2012). Ultraviolet-radiation-induced methane emissions from meteorites and the Martian atmosphere. *Nature*, *486*(7401), 93–96. https://doi.org/10.1038/nature11203

Klusman, R. W., Luo, Y. C., Chen, P., Mischna, M. A., and Yung, Y. L. (2024). Short-term variation in Mars atmospheric methane concentrations driven by barometric pumping. *Icarus*, *408*, 115810. https://doi.org/10.1016/j.icarus.2023.115810

Korablev, O., Vandaele, A. C., Montmessin, F., Fedorova, A. A., Trokhimovskiy, A., Forget, F., Lefèvre, F., Daerden, F., Thomas, I. R., … The ACS and NOMAD Science Teams. (2019). No detection of methane on Mars from early ExoMars Trace Gas Orbiter observations. *Nature*, *568*(7753), 517–520. https://doi.org/10.1038/s41586-019-1096-4

Lefèvre, F., and Forget, F. (2009). Observed variations of methane on Mars unexplained by known atmospheric chemistry and physics. *Nature*, *460*(7256), 720–723. https://doi.org/10.1038/nature08228

Luo, Y., Mischna, M. A., Lin, J. C., Fasoli, B., Cai, X., and Yung, Y. L. (2021). Mars methane sources in northwestern Gale Crater inferred from back trajectory modeling. *Earth Space Sci.*, *8*(11), e2021EA001915. https://doi.org/10.1029/2021EA001915

Moores, J. E., Smith, C. L., and Schuerger, A. C. (2017). UV production of methane from surface and sedimenting IDPs on Mars in light of REMS data and with insights for TGO. *Planet. Space Sci.*, *147*, 48–60. https://doi.org/10.1016/j.pss.2017.09.008

Moores, J. E., Gough, R. V., Martinez, G. M., Meslin, P. Y., Smith, C. L., Atreya, S. K., Mahaffy, P. R., Newman, C. E., and Webster, C. R. (2019a). Methane seasonal cycle at Gale Crater on Mars consistent with regolith adsorption and diffusion. *Nat. Geosci.*, *12*(5), 321–325. https://doi.org/10.1038/s41561-019-0313-y

Moores, J. E., King, P. L., Smith, C. L., Martinez, G. M., Newman, C. E., Guzewich, S. D., Meslin, P. Y., Webster, C. R., Mahaffy, P. R., … Schuerger, A. C. (2019b). The methane diurnal variation and microseepage flux at Gale Crater, Mars as constrained by the ExoMars trace gas orbiter and curiosity observations. *Geophys. Res. Lett.*, *46*(16), 9430–9438. https://doi.org/10.1029/2019GL083800

Mumma, M. J., Villanueva, G. L., Novak, R. E., Hewagama, T., Bonev, B. P., DiSanti, M. A., Mandell, A. M., and Smith, M. D. (2009). Strong release of methane on Mars in northern summer 2003. *Science, 323*(5917), 1041-1045. https://doi.org/10.1126/science.1165243

Pathak, J., Michelangeli, D. V., Komguem, L., Whiteway, J., and Tamppari, L. K. (2008). Simulating Martian boundary layer water ice clouds and the lidar measurements for the Phoenix mission. *J. Geophys. Res.: Planets*, *113*(E3), E00A05. https://doi.org/10.1029/2007JE002967

Peng, S. S., Lin, X., Thompson, R. L., Xi, Y., Liu, G., Hauglustaine, D., Lan, X., Poulter, B., Ramonet, M., … Ciais, P. (2022). Wetland emission and atmospheric sink changes explain methane growth in 2020. *Nature, 612*(7940), 477–482. https://doi.org/10.1038/s41586-022-05447-w

Poling, B. E., Prausnitz, J. M., and O'Connell, J. P. (2001). *The Properties of Gases and Liquids* (5th ed). New York: McGraw-Hill.

Rottman, G. (2005). The SORCE mission. In G. Rottman, et al. (Eds.), *The Solar Radiation and Climate Experiment (SORCE)* (pp. 7–25). New York: Springer. https://doi.org/10.1007/0-387-37625-9_2

Schuerger, A. C., Moores, J. E., Clausen, C. A., Barlow, N. G., and Britt, D. T. (2012). Methane from UV-irradiated carbonaceous chondrites under simulated Martian conditions. *J. Geophys. Res.: Planets*, *117*(E8), E08007. https://doi.org/10.1029/2011JE004023

Stoker, C. R., and Bullock, M. A. (1997). Organic degradation under simulated Martian conditions. *J. Geophys. Res.: Planets*, *102*(E5), 10881–10888. https://doi.org/10.1029/97JE00667

Taylor, P. A., Li, P. Y., Michelangeli, D. V., Pathak, J., and Weng, W. S. (2007). Modelling dust distributions in the atmospheric boundary layer on Mars. *Bound.-Layer Meteor.*, *125*(2), 305–328. https://doi.org/10.1007/s10546-007-9158-9

Thomas, N., Pommerol, A., Hauber, E., Portyankina, G., Tirsch, D., Schmidt, F., Cesar, C., Valantinas, A., Bickel, V. T., and Munaretto, G. (2025). Seasonal and short timescale changes on the Martian surface: Multi-spacecraft perspectives. *Space Sci. Rev.*, *221*(1), 3. https://doi.org/10.1007/s11214-024-01128-4

Thompson, M. A., Krissansen-Totton, J., Wogan, N., Telus, M., and Fortney, J. J. (2022). The case and context for atmospheric methane as an exoplanet biosignature. *Proc. Natl. Acad. Sci. USA*, *119*(14), e2117933119. https://doi.org/10.1073/pnas.2117933119

Vicente-Retortillo, Á., Martínez, G. M., Renno, N. O., Lemmon, M. T., and De La Torre-Juárez, M. (2017). Determination of dust aerosol particle size at Gale Crater using REMS UVS and Mastcam measurements. *Geophys. Res. Lett.*, *44*(8), 3502–3508. https://doi.org/10.1002/2017GL072589

Vicente-Retortillo, A., Martínez, G. M., Rennó, N. O., Lemmon, M. T., de la Torre-Juárez, M., and Gómez-Elvira, J. (2020). In situ UV measurements by MSL/REMS: Dust deposition and angular response corrections. *Space Sci. Rev.*, *216*(5), 97. https://doi.org/10.1007/s11214-020-00722-6

Webster, C. R., Mahaffy, P. R., Atreya, S. K., Flesch, G. J., Mischna, M. A., Meslin, P. Y., Farley, K. A., Conrad, P. G., Christensen, L. E., … The MSL Science Team. (2015). Mars methane detection and variability at Gale crater. *Science*, *347*(6220), 415–417. https://doi.org/10.1126/science.1261713

Webster, C. R., Mahaffy, P. R., Atreya, S. K., Moores, J. E., Flesch, G. J., Malespin, C., Mckay, C. P., Martinez, G., Smith, C. L., … Vasavada, A. R. (2018). Background levels of methane in Mars' atmosphere show strong seasonal variations. *Science*, *360*(6393), 1093–1096. https://doi.org/10.1126/science.aaq0131

Webster, C. R., Mahaffy, P. R., Pla-Garcia, J., Rafkin, S. C. R., Moores, J. E., Atreya, S. K., Flesch, G. J., Malespin, C. A., Teinturier, S. M., … Vasavada, A. R. (2021). Day-night differences in Mars methane suggest nighttime containment at Gale crater. *Astron. Astrophys.*, *650*, A166. https://doi.org/10.1051/0004-6361/202040030